Supplemental Material
A Two-Kind-Boson Mixture Honeycomb Hamiltonian of Bloch Exciton-Polaritons

Haining Pan,[1,2] K. Winkler,[3] Mats Powlowski,[1,4] Ming Xie,[5] A. Schade,[3] M. Emmerling,[3] M. Kamp,[3] S. Klembt,[3] C. Schneider,[3] Tim Byrnes,[6,7,8,9] S. Höfling,[3,10] and Na Young Kim[1,4,11,12,*]

[1]*Institute for Quantum Computing, University of Waterloo, 200 University Ave. West, Waterloo, ON, N2L 3G1, Canada*
[2]*Department of Physics, University of Maryland, College Park, 20740, MD, USA*
[3]*Technische Physik, Physikalisches Institut, Universität Würzbug, D-97074 Würzburg, Germany*
[4]*Department of Electrical and Computer Engineering, University of Waterloo, 200 University Ave. West, Waterloo, ON, N2L 3G1, Canada*
[5]*Department of Physics, The University of Texas at Austin, Austin, TX 78712, USA*
[6]*State Key Laboratory of Precision Spectroscopy, School of Physical and Material Sciences, East China Normal University, Shanghai 200062, China*
[7]*New York University Shanghai, 1555 Century Ave., Pudong, Shanghai 200122, China*
[8]*NYU-ECNU Institute of Physics at NYU Shanghai, 366 Zhongshan Road North, Shanghai 200062, China*
[9]*Department of Physics, New York University, New York, NY 10003, USA*
[10]*School of Physics and Astronomy, University of St. Andrews, St. Andrews, KY16 9SS, United Kingdom*
[11]*Department of Physics and Astronomy, University of Waterloo, 200 University Ave. West, Waterloo, ON, N2L 3G1, Canada*
[12]*Department of Chemistry, University of Waterloo, 200 University Ave. West, Waterloo, ON, N2L 3G1, Canada*

(Dated: August 22, 2018)

PACS numbers: 71.36.+c,78.67.-n, 73.20.At

1. Samples and Experimental Setup

The wafer in this study is composed of two stacks of four 7 nm-thick GaAs quantum-wells embedded in a $\lambda/2$-AlAs cavity structure sandwiched by 32-pair top and 37-pair bottom distributed Bragg reflectors, alternating AlAs and $Al_{0.2}Ga_{0.8}As$ layers. The spatial cavity length variations over the wafer modify detuning values Δ from -18.2 meV to 7.1 meV in our sample. Each site is circular shaped, whose diameter is designed to be fixed at 2 μm and whose etching depth is set to be 5 nm. The resulting sample schematic is sketched in Fig. S1(a). The site-to-site distance d of the neighboring sites has values of 3 and 4 μm, and each block for a specific d has the size of a 150 μm-by-150 μm.

The sample is cooled down to 4 - 6 K, and is excited by a continuous-wave laser at the fixed wavelength 1.616 eV (767.205 nm) at the angle of 60-degrees. Our detection is not polarization-selective. We keep the laser power to be 0.1 - 1 mW, which is much lower than the threshold pump power values 40 - 60 mW at various detuning positions. The laser spot is oval-shaped due to the finite-angle pumping scheme with a size of about 120 μm-by-60 μm.

The standard angle-resolved photoluminescence spectroscopy allows us to map the bandstructures of the honeycomb lattice in the extended zone scheme, and its folded-zone representation is presented in Fig. S1(b) along the three high-symmetry points (Γ, K, M) drawn in Fig. 1(b) of the main text.

2. Bandstructure Calculation

We have shown in the main text about the different results of complete Hamiltonian and approximated Hamiltonian. The distinction is severely bigger in the blue-detuned case; however, in the red-detuned limit ($\Delta \ll 0$), the complete Hamiltonian presented above can be further approximated to a simpler single-component exciton-polariton Hamiltonian(Fig. S2(a)-(h)).

We first define an effective potential strength V_{eff}, which exhibits the spatial variations at different Δ values,

$$V_{\text{eff}} = |C|^2 V_0.$$

*Electronic address: nayoung.kim@uwaterloo.ca

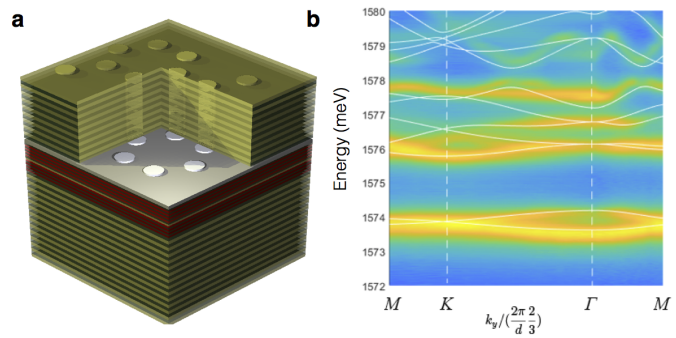

FIG. S1: (a) An illustration of prepared honeycomb lattices patterned by the etching-overgrowth method. Each site is addressed as a circular disk, whose lithographic diameter is 2 μm and etching height is approximately 5 nm. (b) A folded representation of multiple Brillouin zones (BZs) taken from experimental data ($\Delta = -18.2$ meV) along the high-symmetry points denoted in Fig. 1(b). The theoretical folded BZs are overlaid on top of the experimental data in white straight lines. Note that the momentums are projected to k_y direction.

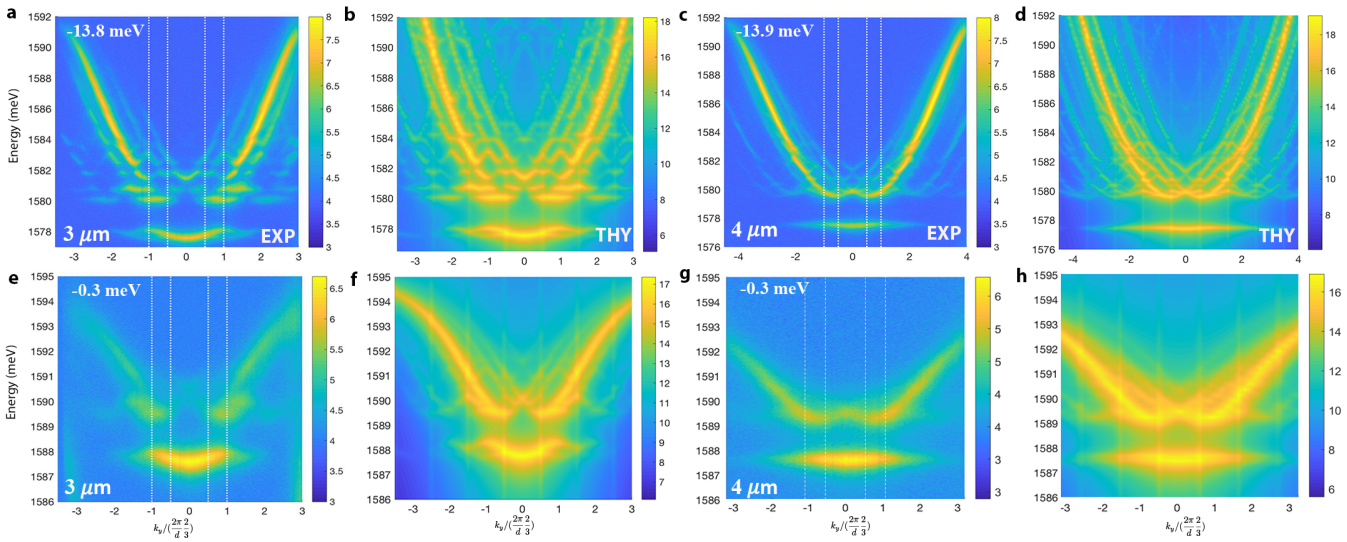

FIG. S2: (a)(c)(e)(g), Cross-sectional energy dispersions along the dashed line 1 in Fig. 1(b) of the main text, passing through $\Gamma - M - \Gamma$. Experimental data for $d = 3$ and 4 μm devices are presented in a log scale of the intensity in (a)(c). Corresponding theoretical bandstructures are computed and presented in a log scale in (b)(d). White vertical lines are drawn at $M = (0, \pm\frac{2\pi}{3d})$ in the first BZ and the $\Gamma = (0, \pm\frac{4\pi}{3d})$ of the second BZ. Experimental (e)(g) and theoretical (f)(h) plots show detuning-value dependent bandstructures of honeycomb lattices. Theoretical bandstructures in (b) and (d) are computed by an approximated Hamiltonian, whereas those of (f) and (h) are from the complete Hamiltonian calculation with two individual components of cavity-photons and quantum-well excitons.

In the extreme red-detuned case, where we have $|C|^2 \sim 1$, the complete Hamiltonian can be approximated to the new Hamiltonian $\boldsymbol{H}_1$,

$$\boldsymbol{H}_1 = \frac{\hbar^2(\boldsymbol{k} + \boldsymbol{k}_{h,h'})^2}{2m_{\text{eff}}} + V_{\text{eff}}(\boldsymbol{k}_{h,h'}) + \varepsilon,$$

where ε is an energy offset value. The proof is as follows: Note that the new Hamiltonian $\boldsymbol{H}_1$ only includes the cavity-photon contribution with the effective mass m_{eff}, namely it has only the half-sized dimension of the complete Hamiltonian $\boldsymbol{H}$. Therefore, we need to extend the space to the same dimension that

$$\tilde{\boldsymbol{H}}_1 = \begin{bmatrix} \boldsymbol{H}_1 & \boldsymbol{0} \\ \boldsymbol{0} & \boldsymbol{0} \end{bmatrix}.$$

Here, if we expand the Fourier series of the potential strength to n-th order $(-n, -n+1, \ldots, n-1, n)$, we have $\boldsymbol{H}_1$

with the $(2n+1)\times(2n+1)$ dimension and $\tilde{\boldsymbol{H}}_1$ with $2(2n+1)\times 2(2n+1)$ dimensions. ($\mathbf{0}$ in above equation stands for the zero matrix). Now the complete Hamiltonian $\boldsymbol{H}$ and the new matrix $\tilde{\boldsymbol{H}}_1$ have the same dimension. The complete Hamiltonian $\boldsymbol{H}$ explicitly reads

$$\boldsymbol{H} = \begin{bmatrix} \boldsymbol{H}_c & \boldsymbol{g_0} \\ \boldsymbol{g_0} & \boldsymbol{H}_X \end{bmatrix},$$

where

$$\boldsymbol{H}_c = \begin{bmatrix} \varepsilon_c + \frac{\hbar^2(\boldsymbol{k}+\boldsymbol{k}_{-n,-n})^2}{2m_c} & \dots & V(\boldsymbol{k}_{(-n,-n),(n,n)}) \\ \vdots & \ddots & \vdots \\ V(\boldsymbol{k}_{(n,n),(-n,-n)}) & \dots & \varepsilon_c + \frac{\hbar^2(\boldsymbol{k}+\boldsymbol{k}_{n,n})^2}{2m_c} \end{bmatrix},$$

$$\boldsymbol{H}_X = \begin{bmatrix} \varepsilon_X + \frac{\hbar^2(\boldsymbol{k}+\boldsymbol{k}_{-n,-n})^2}{2m_X} & \dots & 0 \\ \vdots & \ddots & \vdots \\ 0 & \dots & \varepsilon_X + \frac{\hbar^2(\boldsymbol{k}+\boldsymbol{k}_{n,n})^2}{2m_X} \end{bmatrix},$$

and $\boldsymbol{g_0}$ is the $(2n+1)\times(2n+1)$ diagonal matrix. Because of the mass of exciton $m_X \gg m_c$, the mass of cavity photon, the exciton kinetic term hardly contributes, consequently, this term just vanishes. By introducing the detuning energy $\Delta(\boldsymbol{k})$, we have $\Delta(k_\parallel = 0) = \varepsilon_c - \varepsilon_X$ (In the latter content, for the simplicity, we just use Δ to denote $\Delta(0)$). Finally, $\boldsymbol{H}_X$ is simplified to

$$\boldsymbol{H}_X = \begin{bmatrix} \varepsilon_X & \dots & 0 \\ \vdots & \ddots & \vdots \\ 0 & \dots & \varepsilon_X \end{bmatrix},$$

and $\boldsymbol{H}_c$ reads

$$\boldsymbol{H}_c = \begin{bmatrix} \varepsilon_X + \Delta + \frac{\hbar^2(\boldsymbol{k}+\boldsymbol{k}_{-n,-n})^2}{2m_c} & \dots & V(\boldsymbol{k}_{(-n,-n),(n,n)}) \\ \vdots & \ddots & \vdots \\ V(\boldsymbol{k}_{(n,n),(-n,-n)}) & \dots & \varepsilon_X + \Delta + \frac{\hbar^2(\boldsymbol{k}+\boldsymbol{k}_{n,n})^2}{2m_c} \end{bmatrix},$$

where ε_c is now replaced with $\varepsilon_X + \Delta$ for all diagonal elements by definition. If we take the component ε_X out of the diagonal elements of matrix, $\boldsymbol{H}$ becomes

$$\boldsymbol{H} = \boldsymbol{\varepsilon}_X + \begin{bmatrix} \tilde{\boldsymbol{H}}_c & \boldsymbol{g_0} \\ \boldsymbol{g_0} & \mathbf{0} \end{bmatrix},$$

where

$$\tilde{\boldsymbol{H}}_c = \begin{bmatrix} \Delta + \frac{\hbar^2(\boldsymbol{k}+\boldsymbol{k}_{-n,-n})^2}{2m_c} & \dots & V(\boldsymbol{k}_{(-n,-n),(n,n)}) \\ \vdots & \ddots & \vdots \\ V(\boldsymbol{k}_{(n,n),(-n,-n)}) & \dots & \Delta + \frac{\hbar^2(\boldsymbol{k}+\boldsymbol{k}_{n,n})^2}{2m_c} \end{bmatrix}.$$

Because of the relations of

$$\frac{1}{m_{\text{eff}}} = \frac{|C|^2}{m_c} + \frac{|X|^2}{m_X} \sim \frac{|C|^2}{m_c},$$

and

$$V_{\text{eff}} = |C|^2 V_0,$$

the complete Hamiltonian $\boldsymbol{H}$ is written as

$$\begin{aligned} \boldsymbol{H} &= \boldsymbol{\varepsilon}_X + \begin{bmatrix} \boldsymbol{\Delta} & \boldsymbol{g_0} \\ \boldsymbol{g_0} & \mathbf{0} \end{bmatrix} + \frac{1}{|C|^2}\begin{bmatrix} \boldsymbol{H}_1 - \boldsymbol{\varepsilon} & \mathbf{0} \\ \mathbf{0} & \mathbf{0} \end{bmatrix} \\ &= \boldsymbol{\varepsilon}_X - \frac{\boldsymbol{\varepsilon}}{|C|^2} + \Delta\begin{bmatrix} \mathbf{1} & \frac{\boldsymbol{g_0}}{\boldsymbol{\Delta}} \\ \frac{\boldsymbol{g_0}}{\boldsymbol{\Delta}} & \mathbf{0} \end{bmatrix} + \frac{1}{|C|^2}\tilde{\boldsymbol{H}}_1. \end{aligned}$$

In the cavity-photon limit ($\Delta \to -\infty$), which is the extreme red-detuned case, we have $|C|^2 \to 1$ and $\frac{g_0}{\Delta} \to 0^-$, yielding that the complete Hamiltonian can be further approximated to

$$\boldsymbol{H} = \begin{bmatrix} \boldsymbol{\varepsilon}_X - \boldsymbol{\varepsilon} + \boldsymbol{\Delta} + \boldsymbol{H}_1 & \mathbf{0} \\ \mathbf{0} & \mathbf{0} \end{bmatrix}.$$

Therefore, if we set $\varepsilon = \varepsilon_X + \Delta$, the complete Hamiltonian $\boldsymbol{H}$ is just the approximated $\tilde{\boldsymbol{H}}$

3. Fitting Techniques

Our strategy to perform a systematic fitting analysis is to define a merit function and minimize it with the help of the simulated annealing algorithm. The merit function η as a function of site-to-site distance d, effective potential V_{eff} and effective mass of exciton-polariton m^* is defined as:

$$\eta(d, V_{\text{eff}}, m) = \sum_{\{i,(k_x,k_y)\}} |E_{\text{thy}}^{i,(k_x,k_y)}(d, V_{\text{eff}}, m) - E_{\text{exp}}^{i,(k_x,k_y)}(d, V_{\text{eff}}, m)|^2,$$

where $E_{\text{thy}}^{i,(k_x,k_y)}(d, V_{\text{eff}}, m)$ is the theoretically computed i-th energy state at (k_x, k_y) in momentum space with fitting parameters d, V_{eff}, and m, whilst $E_{\text{exp}}^{i,(k_x,k_y)}(d, V_{\text{eff}}, m)$ are the corresponding experimental data. We sample several characteristic target points from experimental data (k_x, k_y), with which we search the optimal set of (d, V_{eff}, m) to reach the target.

4. Linewidth Information

The theoretical bandstructures presented in Fig. 2 of the main text contain the spectral and momentum linewidth information from experimental bandstructures. Figure S3 shows representative data of linewidth extractions in energy and momentum from a $d = 3$ μm device at $\Delta = -9.6$ meV. The energy plot fits well with the Lorentzian equation (Fig. S3(a)), whereas the momentum cross-sectional plot works well with the Gaussian-shape fit (Fig. S3(b)). The overall intensity of the plot in the whole range at the momentum $\boldsymbol{k}$ and the energy E is given by

$$I(E, \boldsymbol{k}) = \sum_i \sum_{\boldsymbol{h}} \sum_{\boldsymbol{k}_0} |a_{\boldsymbol{h}}^i(\boldsymbol{k})|^2 \frac{\exp - \left(\frac{\boldsymbol{k} - (\boldsymbol{k}_0 + \boldsymbol{h}\cdot\boldsymbol{b})}{\gamma_k}\right)^2}{|E - E_i(\boldsymbol{k})|^2 + \gamma^2},$$

with the energy and momentum relaxation rates γ, γ_k, respectively for the i-th energy state. $a_{\boldsymbol{h}}^i$ indicates component of eigenstate which corresponds $k_{\boldsymbol{h}}$ in the i-th energy state, where $\boldsymbol{h} = (h_1, h_2)$ is the Fourier expansion order, h_1 and h_2 varying from $(-n, -n+1, ..., n-1, n)$. $\boldsymbol{b}$ is the reciprocal unit vector. $\boldsymbol{b} = (b_1, b_2) = \left(\left(0, \frac{4\pi}{3d}\right), \left(\frac{2\pi}{\sqrt{3}d}, -\frac{2\pi}{3d}\right)\right)$ where d is site-to-site distance. $\boldsymbol{k}_0$ are the reference points taken from the experimental energy-dispersion relations, which are uniformly distributed in the first Brillouin zone (BZ). We typically take 25 points in each BZ in order to prevent the coarse granularities.

5. Tight-Binding model theory and the fitting for t and t'

The standard tight-binding (TB) model is adopted from the energy band structure calculation of graphene to extract the two dominant hopping integrals of Bloch exciton-polaritons in the honeycomb lattice potentials (Ref. [12] of the main text). We consider the nearest-neighbor hopping integral t and next-nearest-neighbor hopping integral in the honeycomb. The corresponding tight-binding Hamiltonian is,

$$H = \sum_j \left(t \sum_{|i-j|=d} c_{Bi}^\dagger c_{Aj} + h.c. + t' \sum_{|i-j|=\sqrt{3}d} c_{Ai}^\dagger c_{Aj} + t' \sum_{|i-j|=\sqrt{3}d} c_{Bi}^\dagger c_{Bj} + E_0 c_j^\dagger c_j \right),$$

where the i in the first term denotes the nearest-neighbor site to j and i in the third and fourth term denote the next-nearest-neighbor site to j, E_0 indicates the on-site energy. The Fourier transformation of c_{Aj} is

$$c_{Aj} = \int_\Omega e^{-i\boldsymbol{k}\cdot\boldsymbol{r_j}} c_{A\boldsymbol{k}} \frac{d\boldsymbol{k}}{(2\pi)^2},$$

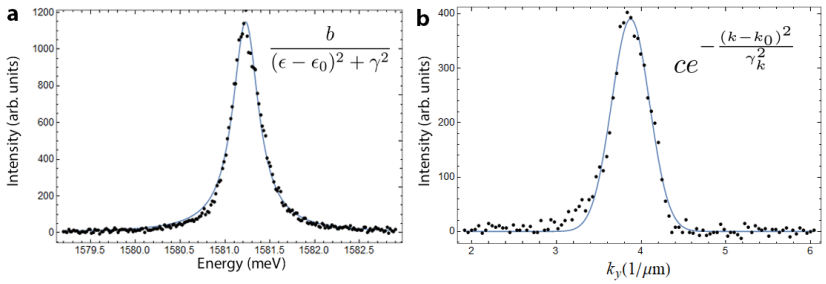

FIG. S3: (a) The Lorentzian model fits our experimental data in the energy axis. The experimental data are taken at Γ. The fitting parameters of this particular plot read $(\epsilon_0, \gamma, b) \rightarrow (1581.23, 0.18, 35.44)$ in unit of (meV, meV, meV^2). (b) The Gaussian model fits our experimental data in the energy axis. The experimental data are taken at where $E = 1591.3$ meV. The fitting parameters of this particular plot read $(c, k_0, \gamma_k) \rightarrow (390.51, 4.02, 0.15)$, where k_0 and γ_k have a unit of $1/\mu$m.

similarly, we can write down the same expression for c_{Bi} and substitute them into the tight-binding Hamiltonian:

$$H = \sum_j t \int \sum_{|i-j|=d} e^{i\boldsymbol{k'}\cdot(\boldsymbol{r_j}+\overrightarrow{AB}_i)-i\boldsymbol{k}\cdot\boldsymbol{r_j}} c^\dagger_{B\boldsymbol{k'}} c_{A\boldsymbol{k}} + h.c. + \sum_{|i-j|=\sqrt{3}d} (E_0 + t' e^{i\boldsymbol{k'}\cdot(\boldsymbol{r_j}+\overrightarrow{AA}_i)-\boldsymbol{k}\cdot\boldsymbol{r_j}})(c^\dagger_{A\boldsymbol{k'}} c_{A\boldsymbol{k}} + c^\dagger_{B\boldsymbol{k'}} c_{B\boldsymbol{k}}) \frac{d\boldsymbol{k}}{(2\pi)^2} \frac{d\boldsymbol{k'}}{(2\pi)^2}.$$

Note that $\sum_j e^{i(\boldsymbol{k'}-\boldsymbol{k})\cdot\boldsymbol{r_j}} = (2\pi)^2 \delta(\boldsymbol{k}-\boldsymbol{k'})$, therefore, the tight-binding Hamiltonian is simplified to

$$H = \begin{pmatrix} c^\dagger_{A\boldsymbol{k}} & c^\dagger_{B\boldsymbol{k}} \end{pmatrix} \begin{pmatrix} E_0 + t' \sum\limits_{|i-j|=d} e^{i\boldsymbol{k}\cdot\overrightarrow{AA}_i} & t \sum\limits_{|i-j|=\sqrt{3}d} e^{i\boldsymbol{k}\cdot\overrightarrow{AB}_i} \\ t \sum\limits_{|i-j|=\sqrt{3}d} e^{-i\boldsymbol{k}\cdot\overrightarrow{AB}_i} & E_0 + t' \sum\limits_{|i-j|=d} e^{i\boldsymbol{k}\cdot\overrightarrow{BB}_i} \end{pmatrix} \begin{pmatrix} c_{A\boldsymbol{k}} \\ c_{B\boldsymbol{k}} \end{pmatrix}.$$

Substituting the nearest-neighbor vector $\overrightarrow{AB}_i = (0, -d), \left(\frac{\sqrt{3}}{2}d, \frac{d}{2}\right), \left(\frac{\sqrt{3}}{2}d, -\frac{d}{2}\right)$ and next-nearest-neighbor vector $\overrightarrow{AA}_i = \overrightarrow{BB}_i = \left(\sqrt{3}d, 0\right), \left(-\sqrt{3}d, 0\right), \left(\frac{\sqrt{3}}{2}d, \frac{3}{2}d\right), \left(\frac{-\sqrt{3}}{2}d, \frac{3}{2}d\right), \left(\frac{\sqrt{3}}{2}d, -\frac{3}{2}d\right), \left(-\frac{\sqrt{3}}{2}d, -\frac{3}{2}d\right)$ and summing them up, we obtain the energies (without loss of generality, we assume t is positive):

$$E = E_0 \pm t\sqrt{3 + f(\boldsymbol{k})} - t' f(\boldsymbol{k}),$$

where

$$f(\boldsymbol{k}) = 2\cos(\sqrt{3}k_x d) + 4\cos\left(\frac{\sqrt{3}}{2}k_x d\right)\cos\left(\frac{3}{2}k_y d\right).$$

In experimental data analysis, we first obtain the energy values at all k_y from the intensity peaks by aforementioned Lorentzian fitting. For the $d = 3$ μm devices, we use a model with two Lorentzian shapes overlapped to find the peaks from the experimental linewidth plots, which inscribes the energy of two states in the s-band. For the $d = 4$ μm devices, we only use one Lorentzian shape to find the s-band because the lower state is mostly populated in the first BZ, whilst the higher state is populated in the second BZ such that can barely be seen in the first BZ.

After the Lorentzian fitting to find the peak, the TB model is applied to fit the four parameters: the offset energy E_0, site-to-site distance d, nearest-neighbor hopping integral t and next-nearest-neighbor hopping integral t'. In addition to the best fitting parameters, we also present (1) standard deviation, which is the average deviation between the experimental point and that fitted point among all momentum k_y; (2) P-value, which can be understood to nullify the hypothesis if P-value $\gtrsim 0.05$, otherwise we can reject the null hypothesis if P-value $\ll 0.05$. We want the small P-value to accept hypothesis such that the fitting model is convincing; (3) error bar, which is set to 95% confidence intervals. The boundary of confidence intervals delimits the error range. For example, Table 1 and Table 2 collect the fitting parameters for the $d = 3$ μm and $d = 4$ μm devices respectively.

	Best Fit	Standard deviation	P-value	Error bar(min)	Error bar(max)
E_0/meV	1577.14	0.003528	2.43E-923	1577.14	1577.15
t/μeV	-92.57	1.321	3.39E-145	-95.18	-89.97
t'/μeV	7.84319	1.01	3.89E-13	-9.84	5.85
d/μm	2.88884	0.020997	6.58E-204	2.84744	2.93024

TABLE I: A red-detuned device of $d = 3$ μm, $\Delta = -14.6$ meV.

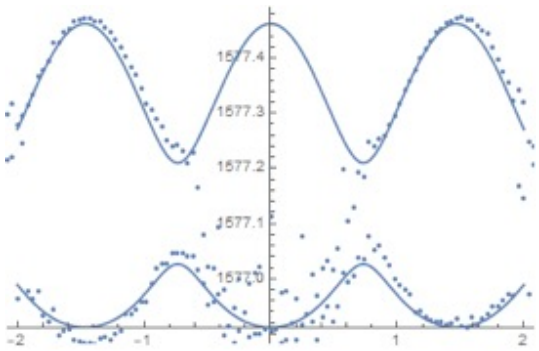

FIG. S4: The fitting model (solid line) and expeirmental peaks (dots) show the agreement. The x-axis is momenum in the unit of $\frac{1}{\mu m}$ and the y-axis is energy in the unit of meV. A red-detuned device of $d = 3$ μm, $\Delta = -14.6$ meV.

	Best Fit	Standard deviation	P-value	Error bar(min)	Error bar(max)
E_0/meV	1582	0.000507	1.48E-556	1582	1582
t/μeV	-9.41	0.197	3.45E-71	-9.8	-9.02
t'/μeV	0.730674	0.141	1.18E-6	0.45	1.011
d/μm	3.72502	0.043485	4.056E-96	3.63876	3.81128

TABLE II: A blue-detuned device of $d = 4$ μm, $\Delta = 8.7$ meV.

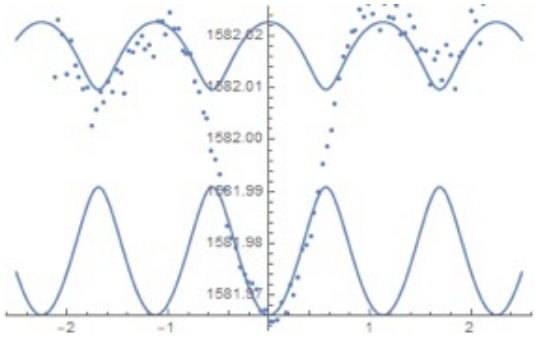

FIG. S5: The fitting model (solid line) and experimental peaks (dots) show the agreement. The x-axis is momenum in the unit of $\frac{1}{\mu m}$ and the y-axis is energy in the unit of meV. A blue-detuned device of $d = 4$ μm, $\Delta = 8.7$ meV.

6. Detuning- and Momentum-dependent potential strength

We summarize the fitting results of V_{eff} and E_0 with our devices. Figure S6(a) plots the photonic potential strength against the fraction of photons $|C|^2$ at $k_{||} = 0$. It exhibits the linear relation, giving the on-average maximum potential height to be 4.98875 meV at $|C|^2 = 1$. In addition, the complete Hamiltonian fitting parameters for potential strength of cavity photon is 5.0169 meV, which are very close to the previous V_0 value, 4.98875 meV. As Δ goes to the positive values, the energy offset approaches the exciton energy which is drawn in the dotted line in Fig. S6(b).

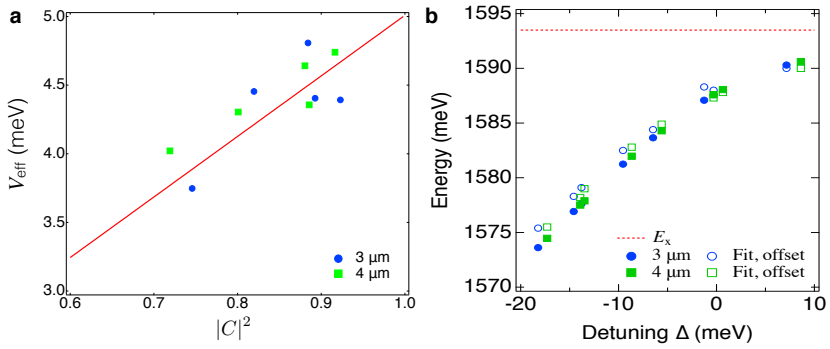

FIG. S6: (a) A linear regression analysis of the photonic-mode potential proportional to the photonic fraction $|C|^2$. (b) The $k_{\|} = 0$ lower-polariton energy and the constant exciton energy (dotted horizontal line) are plotted against Δ values.

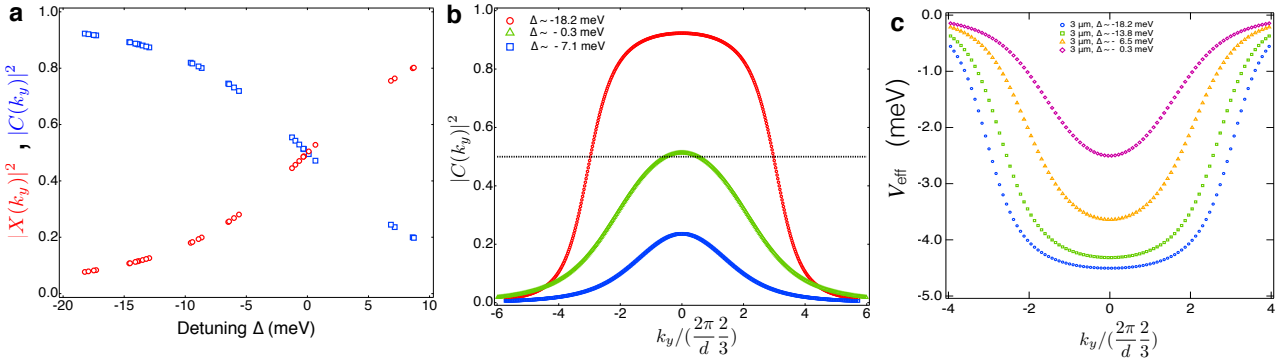

FIG. S7: The computed variations of the $k_{\|} = 0$ exciton ($|X|^2$)and photon ($|C|^2$) fractions and momentum-dependent effective potentials. (a) The relation between $|C|^2$ and $|X|^2$, with respect to Δ. (b) The dispersion of $|C|^2$ in terms of momentum k_y at three different Δ values. (c) The different effective potentials in terms of momentum k_y for the same d but different Δ. (d) The momentum-dependent effective potential for different d values in $\Delta \sim -18$ meV.

We control the mixing amount of excitons and cavity-photons by detuning values (Δ), and we compute their values ($|X|^2, |C|^2$). Figure S7 presents the ratios of $|X|^2$ and $|C|^2$ of all devices at $k_{\|} = 0$. At given Δ, $|X|^2$ and $|C|^2$ are $k_{\|}$-dependent. In consequence, V_{eff} is Δ-dependent as well. As a mixture of the exciton and the cavity-photon, exciton-polaritons have distinct energy-momentum relations. Since fractions of exciton and photons are momentum-dependent, the potential profiles are not constant in the momentum space. Figure S7(c) presents the calculated momentum-space potential profiles at different Δ of $d = 3$ μm devices and at different d values at similar Δ-values. The more blue-detuned devices, the potential height is reduced at $k_{\|} = 0$, and the potential shape is smoothened in the $k_{\|}$values and approaches to 0 rapidly in non-zero $k_{\|}$ values. This explains the flattened polariton-like dispersions appear in large $k_{\|}$-values more vividly in the blue-detuned device.